

Machine Learning Calculation Model for Hydrodynamic Lubrication Characteristics of a Miter Gate Bottom Pivot

Xiang Xu ^{1,2}, Zhengguo Guan ^{1,2}, Zhixiong Li ³, Maciej Sulowicz ⁵, Grzegorz Królczyk⁴, Tiancan Dai ^{1,2} and Xinze Zhao ^{1,2}

¹ College of Mechanical and Power Engineering, China Three Gorges University, Yichang 443002, China

² Hubei Key Laboratory of Hydroelectric Machinery Design & Maintenance, China Three Gorges University, Yichang 443002, China

³ Faculty of Mechanical Engineering, Opole University of Technology, Opole 45-758, Poland

⁴ Department of Electrical Engineering, Cracow University of Technology, Cracow 31-155, Poland

* Correspondence: z.li@po.edu.pl

Abstract: The bottom pivot is a vital support device in the miter gate but often subject to poor lubrication and wear failures. Calculating the hydrodynamic lubrication characteristics of the bottom pivot is a complex three-dimensional (3D) problem, and most of existing models adopt simplified assumptions to reduce the calculation difficulty. To solve this issue, this work develops a 3D model to calculate the hydrodynamic lubrication characteristics of the miter gate bottom pivot. The finite difference method is used to solve the oil film thickness and pressure distribution based on the spherical coordinates Reynolds equation. The component forces in three directions are calculated from the pressure distribution and compared with the theoretical values to generate the calculation difference. Then, the genetic algorithm (GA) is used to minimize the difference to determine the optimal initial parameters for the 3D model. The analysis results show that the calculation accuracy can be significantly improved by using the optimal initial model parameters. **When our initial pressure is 5.64MPa, the results meet the engineering accuracy requirements.**

Keywords: miter gate; bottom pivot; hydrodynamic lubrication; genetic algorithm

Nomenclature

h	oil films thickness
μ	dynamic viscosity of lubricating medium
p	oil film pressure
\bar{U}	relative movement speed of the friction pair
t	time
R	distance from the point of the origin
θ, ϕ	spherical coordinates
τ	shear stress
$\varepsilon_x, \varepsilon_y, \varepsilon_z$	eccentricity of the spherical bearing
$\omega_x, \omega_y, \omega_z$	relative rotational angular velocity
τ_0	ultimate dynamic shear stress
c	clearance of friction pair

1. Introduction

Currently, a large number of miter gates suffer from structural damages due to excessive bottom pivot wear [1]. As an important supporting component for the miter gate, the bottom pivot works in a harsh underwater environment and is prone to wear failures. Daniel [2] found excessive wear on the miter gate bottom pivot in the Dutch navigation locks while Zhao et al. [3] suggested that it is crucial to measure the surface wear of the bottom pivots to prevent unexpected failures and prolong the service life of the pivots. Xiaoxue Wu[4] improved the data set, changed the noisy data set into a clean data set, and then applied it to the security vulnerability report (SBR), and the prediction effect is much better than before. Sheng Chunfu[5] Taking ultra high molecular weight polyethylene (UHMWPE) fiber as the research object, they discussed the effects of wear frequency and yarn tension on its wear life. Ning Fanggang[6] proposed a method of using functional graphene / polyurethane composite coating (FG / PU) to improve the wear resistance of yarn to high modulus polyethylene fiber (HMPE) yarn.

Due to unique structural features, the mathematical model of the bottom pivot can be simplified as a spherical bearing model. The lubrication characteristics of the bottom pivot can be analyzed by the spherical bearing lubrication. Pylos et al. [7] predicted the possible lubrication states of the wrist implants in the spherical bearing surface and the minimum oil film thickness under different working conditions using the elastohydrodynamic (EHD) lubrication theory. Deng et al. [8] used the Reynolds equation in spherical coordinates to inspect the lubrication of the bearing ball. Agrawal [9] added micro texture on the surface of the hybrid spherical thrust bearing and solved the modified Reynolds equation by finite element method. Wang and Sharma [10] solved the steady-state Reynolds equation on the spherical bearing using the finite difference method and relaxation iteration method. Kumar et al. [11] used the deterministic theory to analyze the influence of the surface roughness on the squeezed film lubrication of the spherical bearing. Huang et al. [12] studied the lubrication of the spherical crown pit texture model under different surface texture distribution parameters using the hydrodynamic lubrication theory. It can be learned from existing publications that the difference method is often used for the iterative solutions for calculating the Reynolds equation, resulting in low accuracy and heavy calculation time. The evolutionary algorithm can address this issue by properly optimizing the initial model parameters in the difference method. Ji Y [13] combined the radial basis function with the NSGA-II genetic algorithm to carry out multi-objective optimization design for the turbine impeller. The efficiency and accuracy of the model has been improved. Tiwari et al. [14-17] used the genetic algorithm for optimum design of rolling bearings and spherical roller bearings. However, investigating the hydrodynamic lubrication characteristics of the bottom pivot using the genetic algorithm optimized finite difference model has not been found yet. It is worth combining them to improve the calculation performance on the hydrodynamic lubrication characteristics of the bottom pivot.

This work develops a genetic algorithm optimized finite difference model to investigate the hydrodynamic lubrication characteristics of the bottom pivot. Firstly, the force on the bottom pivot is calculated through theoretical analysis. Then, the initial model parameters are used to solve the Reynolds equation in the spherical coordinate, so as to obtain the film thickness and pressure distribution of the bottom pivot. Then the calculated results are compared with theoretical values, and the difference is used as the feedback information to optimize the initial parameters using the genetic algorithm. Changes in oil film and pressure of the pivot after parameters optimization are studied under different operation conditions. In this paper, a method combining finite difference method and genetic algorithm is proposed to solve the Reynolds equation. In the process of solving, there is no need to deal with the Reynolds equation dimensionless, but only need to replace the actual parameters. The model used can be applied to the solution of Reynolds equation in different cases, and the difference is less than 1.0×10^{-3} .

The remainders of this paper are organized as follows: theoretical model of the pivot is established in section 2 and the finite difference model is introduced in section 3. Section 4 presents the optimization procedure of the genetic algorithm. The numerical calculation results are analyzed in Section 5. The main conclusions are drawn in section 6.

2. Mathematical model of a bottom pivot

The general form of the Reynolds equation is:[18]

$$\nabla \cdot \left(\frac{h^3}{12\mu} \nabla p \right) = \nabla \cdot (h\bar{\mathbf{U}}) + \frac{\partial h}{\partial t} \quad (1)$$

where h is the oil films thickness; μ is the dynamic viscosity of lubricating medium; P is oil film pressure; $\bar{\mathbf{U}}$ is the relative movement speed of the friction pair; t is the time.

Replace x, y and z in the rectangular coordinates with θ and ϕ in the spherical coordinates, it yields

$$\begin{cases} x = R \sin \theta \sin \phi \\ y = R \sin \theta \cos \phi \\ z = R \cos \theta \end{cases} \quad (2)$$

where R is the distance from the point of the origin; θ is the angle between the point and z-axis. ϕ is the angle between the projection of this point in the XY plane and the Z-axis.

The bottom pivot is lubricated with grease, and its lubricating medium can be considered as a Bingham fluid, so the shear stress τ can be expressed as

$$\tau = \tau_s + \eta \frac{\partial \mathbf{v}}{\partial \delta} \quad (3)$$

where τ_0 is the ultimate dynamic shear stress.

Due to high viscosity of the lubricant grease and small gap between the bottom pivots, the grease flow can be considered as a laminar flow. The classical Reynolds equation can be derived from the Navier-Stokes equations if ignoring the curvature of the fluid film, inertial force and slip boundary. The Reynolds equation of the incompressible fluid in the spherical coordinates can be obtained as follows [18]:

$$\begin{aligned} & \frac{1}{R^2} \left[\frac{1}{\sin \theta} \frac{\partial}{\partial \theta} \left(\frac{h^3}{12\mu} \sin \theta \frac{\partial p}{\partial \theta} \right) + \frac{1}{\sin^2 \theta} \frac{\partial}{\partial \phi} \left(\frac{h^3}{12\mu} \frac{\partial p}{\partial \phi} \right) \right] \\ &= \frac{1}{R \sin \theta} \left(h \cos \theta \bar{U}_\theta + h \sin \theta \frac{\partial \bar{U}_\theta}{\partial \theta} + h \frac{\partial \bar{U}_\phi}{\partial \phi} + \bar{U}_\theta \sin \theta \frac{\partial h}{\partial \theta} + \bar{U}_\phi \frac{\partial h}{\partial \phi} \right) + \frac{\partial h}{\partial t} \end{aligned} \quad (4)$$

where, \bar{U}_θ and \bar{U}_ϕ are the linear velocity of the fluid in θ and ϕ directions, and R is the radius of the base pivot.

Using ε_x , ε_y and ε_z to represent the eccentricity of the spherical bearing and ω_x , ω_y and ω_z to represent the relative rotational angular velocity, we can get

$$h = c(1 - \varepsilon_x \sin \theta \cos \phi - \varepsilon_y \sin \theta \sin \phi - \varepsilon_z \cos \theta) \quad (5)$$

$$\bar{U}_\theta = \frac{-R\omega^x \sin \phi + R\omega^y \cos \phi}{2} \quad (6)$$

$$\bar{U}_\phi = \frac{-R\omega^x \cos \phi \cos \theta - R\omega^y \sin \phi \cos \theta + R\omega^z \sin \theta}{2} \quad (7)$$

where c to represent the clearance of friction pair,

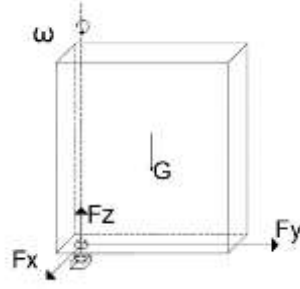


Figure 1. Brief structure drawing of miter gate

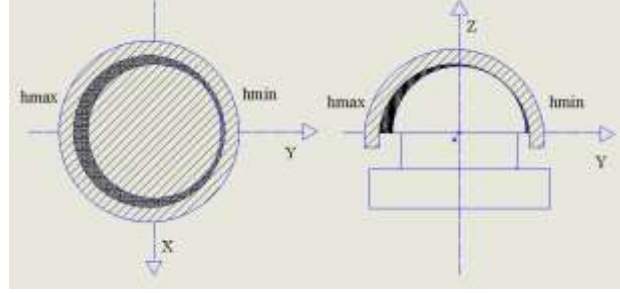


Figure 2. Schematic diagram of oil film thickness distribution (vertical view & front view)

The miter gate structure is shown in Figure 1 and the oil film distribution is depicted in Figure 2. The bearing capacity of the bottom pivot is calculated as followings:

$$\begin{cases} F^x = R^2 \int_{\phi_1}^{\phi_2} \int_{\theta_1}^{\theta_2} p \sin \theta \cos \phi \sin \theta d\theta d\phi \\ F^y = R^2 \int_{\phi_1}^{\phi_2} \int_{\theta_1}^{\theta_2} p \sin \theta \sin \phi \sin \theta d\theta d\phi \\ F^z = R^2 \int_{\phi_1}^{\phi_2} \int_{\theta_1}^{\theta_2} p \cos \theta \sin \theta d\theta d\phi \end{cases} \quad (8)$$

Based on Figure 2, Eq. (3) is processed and simplified to obtain Eq. (9):

$$\begin{aligned} & \frac{3hh'_\theta + h^3}{12\mu R^2} \frac{\partial^2 p}{\partial \theta^2} + \frac{h^3}{12\mu R^2 \sin^2 \theta} \frac{\partial^2 p}{\partial \phi^2} + \frac{h^3}{12\mu R^2} \frac{\cos \theta}{\sin \theta} \frac{\partial p}{\partial \theta} + \frac{3hh'_\phi + h^3}{12\mu R^2 \sin^2 \theta} \frac{\partial p}{\partial \phi} \\ &= \frac{1}{R \sin \theta} \left(h \cos \theta \overline{U}_\theta + h \sin \theta \frac{\partial \overline{U}_\theta}{\partial \theta} + h \frac{\partial \overline{U}_\phi}{\partial \phi} + \overline{U}_\theta \sin \theta \frac{\partial h}{\partial \theta} + \overline{U}_\phi \frac{\partial h}{\partial \phi} \right) + \frac{\partial h}{\partial t} \end{aligned} \quad (9)$$

For the convenience of calculation, Eq. (9) can be reduced as

$$A \frac{\partial^2 p}{\partial \theta^2} + B \frac{\partial^2 p}{\partial \phi^2} + C \frac{\partial p}{\partial \theta} + D \frac{\partial p}{\partial \phi} = E \quad (10)$$

The coefficients in Eq. (10) are described as

$$\left\{ \begin{array}{l} A = \frac{h^3}{12\mu R^2} \\ B = \frac{h^3}{12\mu R^2 \sin^2 \theta} \\ C = \frac{h^3 \cos \theta + 3h^2 h'_\theta \sin \theta}{12\mu R^2 \sin \theta} \\ D = \frac{3h^2 h'_\phi}{12\mu R^2 \sin^2 \theta} \\ E = \frac{1}{R \sin \theta} \left(h \cos \theta \overline{U}_\theta + h \sin \theta \frac{\partial \overline{U}_\theta}{\partial \theta} + h \frac{\partial \overline{U}_\phi}{\partial \phi} + \overline{U}_\theta \sin \theta \frac{\partial h}{\partial \theta} + \overline{U}_\phi \frac{\partial h}{\partial \phi} \right) \end{array} \right. \quad (11) \quad 123$$

3. Numerical Analysis

The finite difference method is used to solve the Reynolds equation, and the difference relationship is described in Figure 3. The solution area is divided into 90 meshes in the direction of θ and 360 meshes in the direction of ϕ . The step length along the θ direction is $\pi R/180$ and the step length along the ϕ direction is $\pi R/180$.

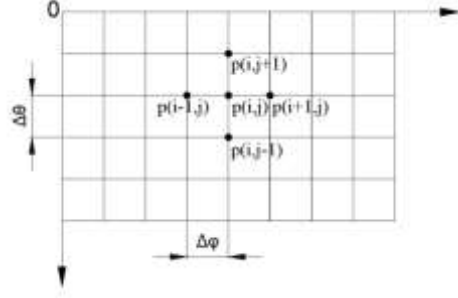


Figure 3. Difference relationship

According to the difference relationship in Figure 3, the partial derivative of the pressure at point (i, j) can be expressed as:

$$\begin{aligned} \left(\frac{\partial p}{\partial \theta} \right)_{i,j} &= \frac{p_{i+1,j} - p_{i-1,j}}{2\Delta\theta} \\ \left(\frac{\partial p}{\partial \phi} \right)_{i,j} &= \frac{p_{i,j+1} - p_{i,j-1}}{2\Delta\phi} \\ \left(\frac{\partial^2 p}{\partial \theta^2} \right)_{i,j} &= \frac{p_{i+1,j} + p_{i-1,j} - 2p_{i,j}}{\Delta\theta^2} \\ \left(\frac{\partial^2 p}{\partial \phi^2} \right)_{i,j} &= \frac{p_{i,j+1} + p_{i,j-1} - 2p_{i,j}}{\Delta\phi^2} \end{aligned} \quad (12) \quad 134$$

Substituting Eq. (12) into Eq. (11), the relation between p of each node and p of adjacent nodes can be obtained as

$$\tilde{p}_{i,j} = C_N p_{i,j+1} + C_S p_{i,j-1} + C_E p_{i+1,j} + C_W p_{i-1,j} + G \quad (13) \quad 137$$

$$\left\{ \begin{array}{l} C_N = \frac{\frac{B}{\Delta\phi^2} + \frac{D}{2\Delta\phi}}{K} \\ C_S = \frac{\frac{B}{\Delta\phi^2} - \frac{D}{2\Delta\phi}}{K} \\ C_E = \frac{\frac{A}{\Delta\theta^2} + \frac{C}{2\Delta\theta}}{K} \\ C_W = \frac{\frac{A}{\Delta\theta^2} - \frac{C}{2\Delta\theta}}{K} \\ G = -\frac{E}{K} \\ K = 2 \left(\frac{A}{\Delta\theta^2} + \frac{B}{\Delta\phi^2} \right) \end{array} \right. \quad (14) \quad 138$$

After the equation is discretized, Jacobi iteration is used to solve the differential equation. 139
140

$$p_{i,j}^{k+1} = (1-\alpha) p_{i,j}^k + \alpha \tilde{p}_{i,j}^k \quad (15) \quad 141$$

Where $p_{i,j}^k$ is the current pressure, $p_{i,j}^{k+1}$ is a new pressure, $\tilde{p}_{i,j}^k$ is the pressure obtained by Eq. (13), and α is the decimal between 0 and 1. 142
143

The boundary was determined by the following well-known scheme: 144

If $p_{i,j} < 0$, $p_{i,j} = 0$ 145

Adopts the discriminant method of relative convergence in the Reynolds Equation, we derive 146
147

$$\frac{\sum_i^n \sum_j^m |p_{i,j}^{k+1} - p_{i,j}^k|}{p_{i,j}^{k+1}} \leq \varepsilon \quad (16) \quad 148$$

where, n is the number of grids divided by rows and m is the number of grids divided by columns, and ε is a small constant; and in this work $\varepsilon = 1.0 \times 10^{-4}$. 149
150

The pressure on the bottom pivot edge is set to zero. In the initial condition, once the pressure is determined, the array of the NumPy library in Python is applied to calculating the component force of each pressure point by multiplying the elements, and then, sum the component forces in each direction as the total component force in this direction. 151
152
153
154

Let us assume that there is only one load in the Z direction and only one rotational angular velocity around the Z-axis. At the beginning of the calculation, the film thickness distribution matrix is calculated by Eq. (5), and the obtained film thickness is substituted for Eq. (11) to calculate the values of A, B, C, D, E. Substitute the computed values into Eqs. (13) and (14) to calculate the pressure distribution matrix; repeat the iterative process of Eq. (13), and then, judge whether the iteration converges on Eq. (15). After convergence, a stable pressure distribution matrix is obtained. During the iterative process, in order to remove the negative pressure, the calculated negative pressure is reset to zero to meet the Reynolds boundary conditions [15] after several iterations in this study. The calculation procedure is shown in Figure 4. 155
156
157
158
159
160
161
162
163
164
165

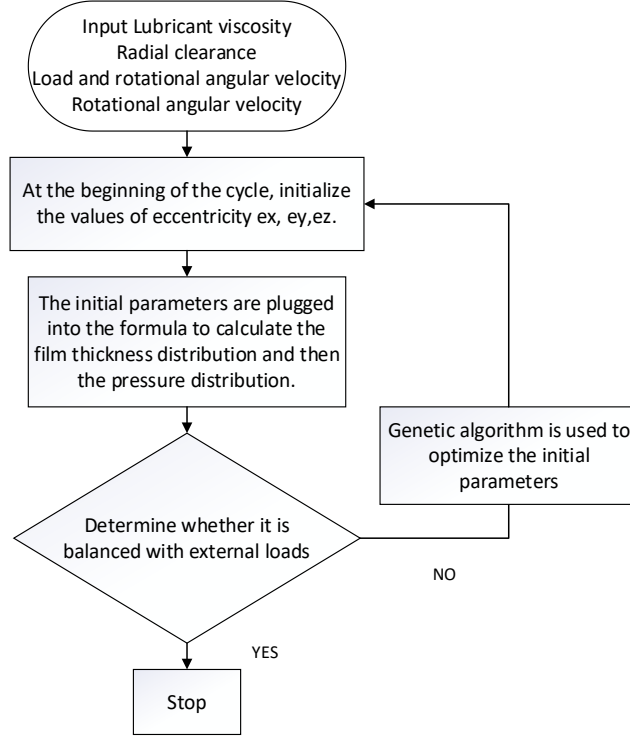


Figure 4. Schematic of the solution process

4. Model Initial Parameters Optimization

Since the component forces calculated by the finite difference method is affected by the initial model parameters, such as the initial pressure and initial eccentricity, the Genetic algorithm (GA) is employed to optimize the initial parameters. Due to complex coupling effect, the relationship between the initial pressure and the force component is non-linear. Thus, a proper objective function is a must for the GA optimization. In this study the objective function is selected as:

$$f(x) = \min(f_z - f'_z) \quad (17)$$

In the above formula, f_z represents the force in the vertical direction and f'_z represents the force calculated by the finite difference method. A random number generating function is used to create 12-bit binary random data to represent as the GA initial "genes". If num is the actual number converted from binary to decimal, it will be mapped into a specified range by

$$X = num \times (X_{\max} - X_{\min}) + X_{\min} \quad (18)$$

When iterating the difference equation, in order to obtain a good "gene", an evaluation information (i.e., the fitness function) is needed, which is expressed as

$$g(x) = -(f(x) - f(x)_{\max}) + 0.0001 \quad (19)$$

After the evaluation information is determined according to Eq. (19), possible solutions will be selected. The solutions closer to the theoretical value are more likely to be retained, and the corresponding probability of selection is higher. Parameter settings of the GA and the pivot are shown in the following tables.

Table 1. GA settings

Parameter	Value
Population	200
Probability of mutation	0.9

The crossover probability	0.1
Evolution generations	40

Table 2. Bottom pivot material and iterative parameters

Parameter	Value
Base pivot mushroom head material	40 Cr
Bottom pivot tile material	QT600-3
Quality of gate	850 t
Lubricant viscosity	645 Pa·s
Elastic modulus of bearing bush	169 GPa
Bearing bush Poisson's ratio	0.286
Tensile strength of bearing bush	≥ 600 MPa
Initial eccentricity	0,0.1,0.1
The iteration error	0.0001
Maximum search times	5000

5. Results and discussion

5.1. The initial pressure

According to the above solving process, the author wrote a Python program to optimize several working conditions. Taking a specific type of gate as an example, the initial parameter Settings of simulation are shown in Table 1 and Table 2. Three-dimensional, two-dimensional, spherical and rectangular images of oil film thickness and pressure distribution are shown as follows:

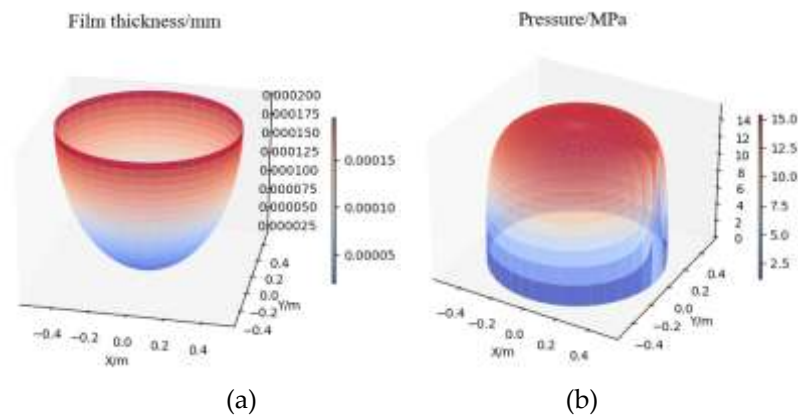


Figure 5. Three dimensional schematic diagram of oil film thickness and pressure distribution

Figure 5 shows that the oil film thickness gradually decreases to the θ direction. Since the initial parameters of the are preset, the oil film thickness along the φ direction will first decrease and then increase.

The normalized results of the maximum stress are shown in Figure 6.

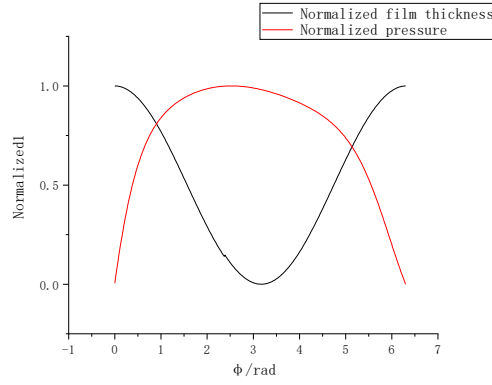


Figure 6. Schematic diagram of the changing trend of normalized pressure and film thickness

According to Eq. (13), during each iteration, the pressure at the center point in the grid plane is affected by the surrounding points. Therefore, different initial pressures will affect the calculation results. Other parameters are shown in Table 2. Tet the initial pressure from 1 MPa, 2 MPa, 3 MPa... to 10 MPa, and observe the impact of different initial pressures on the results. The results are shown in the following figure:

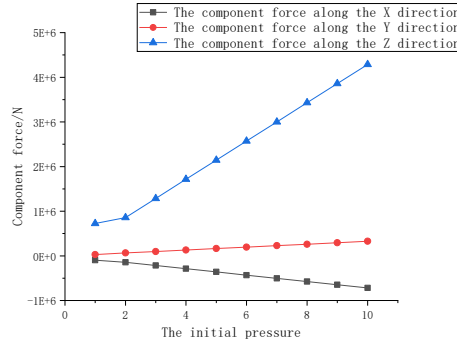
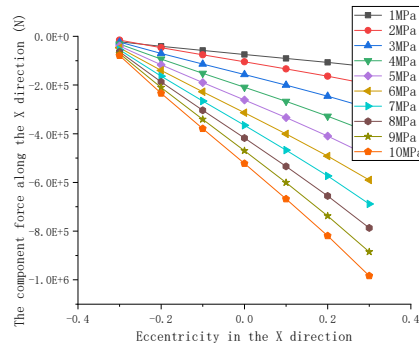


Figure 7. The effect of the initial pressure on the result of the force-splitting calculation

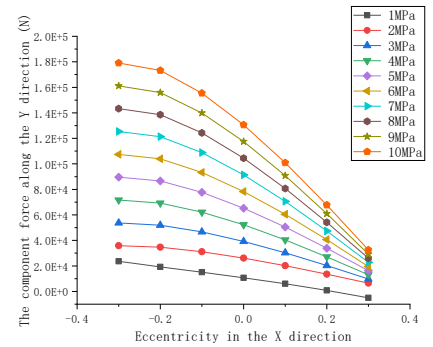
As can be seen from Figure 7, the initial pressure and the relationship between components is a linear approximation, the increase of initial pressure to the element of different direction is different. Therefore, when calculating the bearing capacity of the bottom pivot, choosing an appropriate initial pressure is conducive to improve the calculation speed.

5.2. Eccentricity

In the actual process, the bottom pivot is affected by external load and its gravity resulting in different eccentricities. That the lubricating oil film produces a wedge effect, affecting the regular operation of the bottom pivot. According to Equation (4), the oil film thickness at any point in the bottom pivot is related to its eccentricity. To analyze the influence of film thickness on the lubrication performance of the bottom pivot, different eccentricity ratios are selected to observe the changes of force components in each direction, as shown in the figure below:



(a)



(b)

207

208

209

210

211

212

213

214

215

216

217

218

219

220

221

222

223

224

225

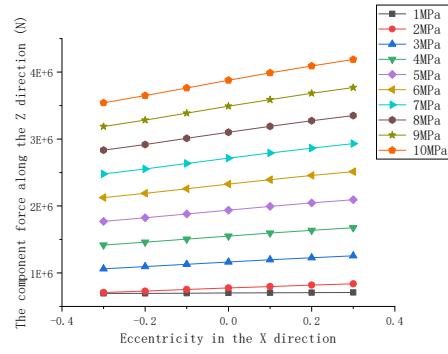
226

227

228

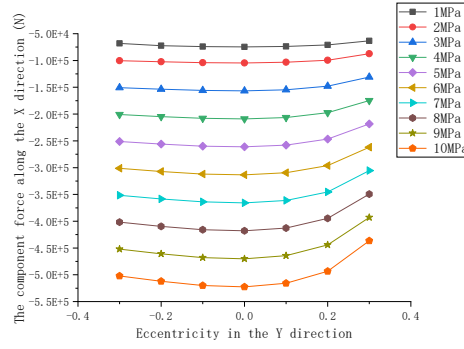
229

230

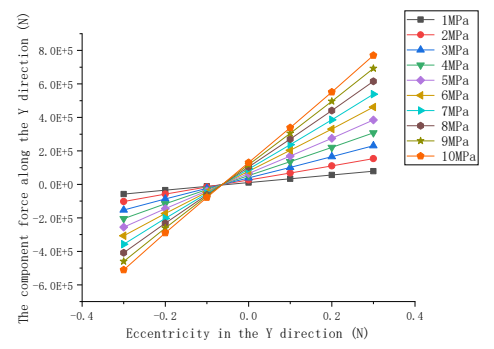


(c)

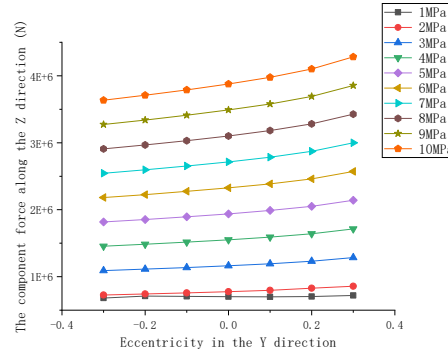
Figure 8. Influence of eccentricity in the X direction on component force under different initial pressures



(a)

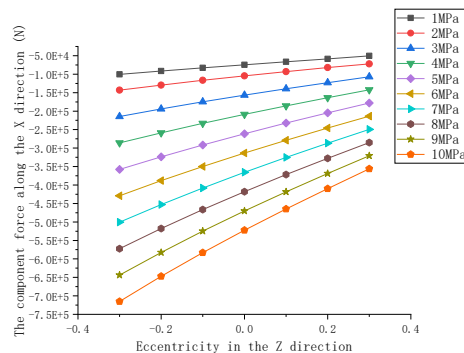


(b)

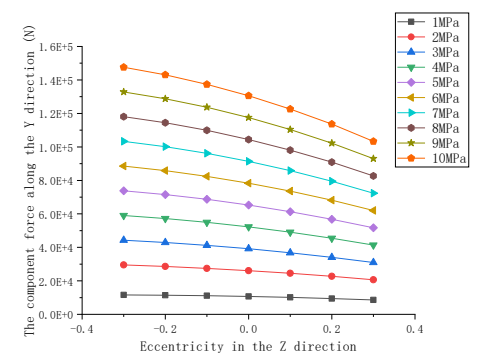


(c)

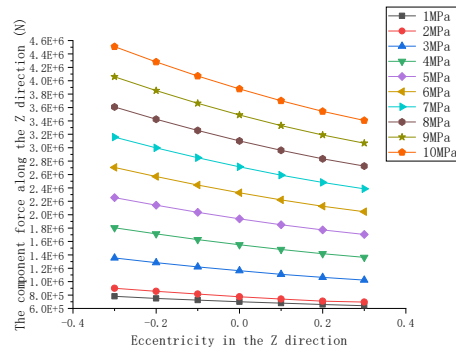
Figure 9. Influence of eccentricity in the Y direction on component force under different initial pressures



(a)



(b)



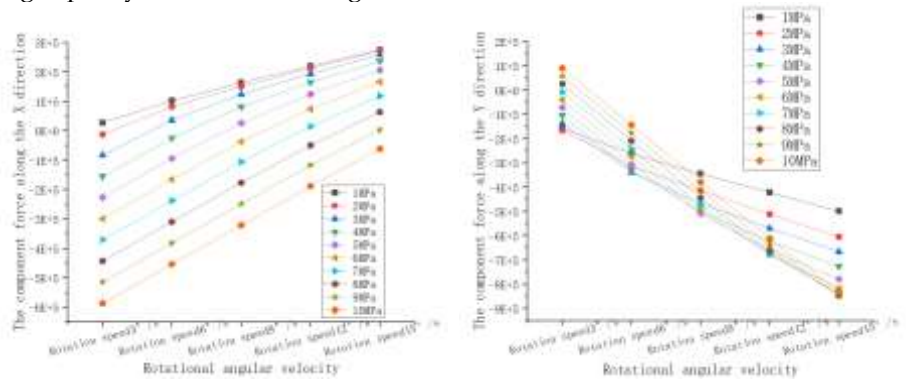
(c)

Figure 10. Influence of eccentricity in the Z direction on component force under different initial pressures

It can be seen from Figure 8, 9, 10 that when the eccentricity in the X direction increases, the bearing capacity in the X and Z directions increases and the bearing capacity in the Y direction decreases. The increase in eccentricity in the Y direction will also lead to the increase in bearing capacity and the greater the initial pressure, the more obvious the impact on bearing capacity. When the eccentricity in the Z direction increases, the bearing capacity of the X direction increases and the bearing capacity of Y and Z directions decreases.

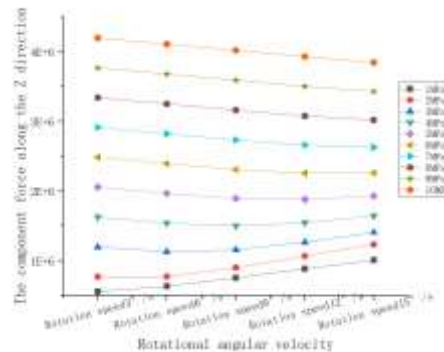
5.3. Rotational angular velocity

When the spherical bearing does not rotate, there is only a static pressure effect. When it turns, the dynamic pressure effect is produced due to the existence of a wedge-shaped oil film, which affects the bearing capacity. Under the condition that other parameters remain unchanged, the rotating speeds are $3^\circ/\text{s}$, $6^\circ/\text{s}$, $9^\circ/\text{s}$, $12^\circ/\text{s}$ and $15^\circ/\text{s}$. the bearing capacity is shown in the figure below.



(a)

(b)



(c)

Figure 11. Influence of rotational speed on component force under different initial pressure

As shown from Figure 11, with the increase of rotating speed, the bearing capacity in the X direction also increases, and the greater the initial pressure, the more obvious the

improvement. But the Y direction is the opposite. When the initial pressure in the Z direction is less than 4MPa, the higher the speed is, the greater the bearing capacity is, but it will decrease when the initial pressure is greater than 4MPa.

5.4. Optimization process analysis

Even if the pressure obtained by the difference method converges, the obtained solution is not necessarily the fundamental solution to the problem, so the feedback processes needs to be used. The parameters of the genetic algorithm are 200 population sizes, 40 number of evolutions, and 0.6 and 0.9 cross probabilities, respectively, and the goal is to minimize the difference between the carrying capacity and the theoretical value of the Z direction. The variation process of the initial pressure in the difference method of the evolution times is shown in the following figure:

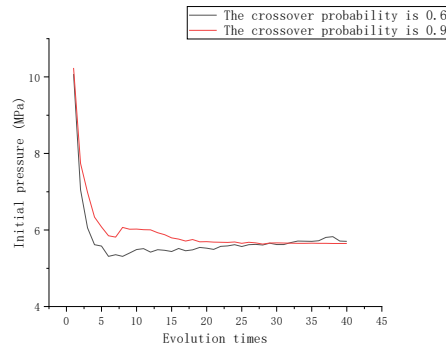


Figure 13. Relationship between evolution times and initial pressure

It can be seen from Figure 13. The initial pressure obtained when the crossover probability is 0.9 gradually tends to be stable after 30 evolutions. In contrast when the crossover probability is 0.6, it will not be stable after 30 changes. Therefore, this paper adopts the crossover probability of 0.9 for optimization.

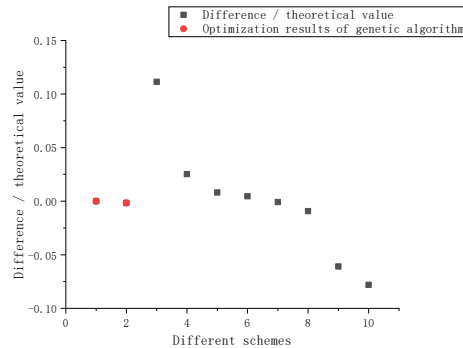


Figure 14. Comparison diagram of optimization results

As can be seen from the above figure, the difference between the calculated value and the theoretical value is quite different to different schemes. Schemes 1 and 2 are the results obtained after genetic algorithm optimization, and schemes 3 to 10 are the results of manually setting the initial value. It can be seen from the figure that the genetic algorithm has higher accuracy, and there is no need to try it many times manually. After GA optimization, when the initial pressure is about 5.64MPa, the ratio of the difference between the estimated value and the hypothetical value of the hypothetical value is less than 1.0×10^{-3} .

6. Conclusions

A numerical calculation model of hydrodynamic lubrication characteristics of miter gate bottom pivot is proposed to this paper. The effects of initial pressure, eccentricity and rotating speed on oil film thickness and pressure distribution are analyzed. In the iterative process, the increase in initial pressure will significantly improve the bearing capacity for the z-axis direction, and the increase in eccentricity in the X and Y directions will increase

the component forces along these directions. The greater the initial pressure, the faster the component increases. At the same time, the increase in Z-direction eccentricity will reduce the bearing capacity. In addition, the component forces in the X and Z directions will increase as the rotation increases. But the elements in the Y direction will decrease. Finally, the genetic algorithm is used to optimize the initial pressure, so that the error between the theoretical value and the calculated value is significantly reduced, and the calculated results and external load meet the engineering accuracy requirements. Through the calculation of finite difference method and genetic algorithm, the oil film thickness distribution and pressure distribution are consistent with the expectation. Because the load on the bottom pivot is large and vertical, the film thickness at the center of the ball is the thinnest and the pressure in this area is the largest. We can use more effective optimization algorithms. When there are more data, we can use machine learning and deep learning to train larger models to improve the accuracy and adaptability of the models.

Funding: The research leading to these results has received funding from the Norwegian Financial Mechanism 2014-2021 under Project Contract No 2020/37/K/ST8/02748.

Conflicts of Interest: The authors declare no conflict of interest.

References

1. Eick B A, Treece Z R, Spencer B F, Smith M D, Sweeney S C, Alexander Q G, Foltz S D. Automated damage detection in miter gates of navigation locks. *Structural Control and Health Monitoring* **2018**, 25 (1).
2. Daniel R. Recent structural developments in miter gates for navigation locks (in English), Inzynieria Morska i Geotechnika (Maritime Engineering and Soil Technology), No. 6/2017, Gdansk, Nov./Dec. 2017. 2018.
3. Xinze Z, Dan S, Xiang X, Yang D, Zhuanghui G. Study on surface wear of gate bottom pivot based on multi-notch measurement. *Wear*, 2020, 462-463.
4. Wu, X., Zheng, W., Xia, X., & Lo, D. (2021). Data Quality Matters: A Case Study on Data Label Correctness for Security Bug Report Prediction. *IEEE transactions on software engineering*, 1. doi: 10.1109/TSE.2021.3063727
5. Sheng Chunfu, He Guifang, Hu Zhongxian, Chou Chiate, Shi Jiangao, Li Jun, Meng Qingjian, Ning Xin, Wang Liming, Ning Fanggang. Yarn on yarn abrasion failure mechanism of ultrahigh molecular weight polyethylene fiber. *Journal of Engineered Fibers and Fabrics*, 2021, 16.
6. Ning Fanggang, He Guifang, Sheng Chunfu, He Hongwei, Wang Jian, Zhou Rong, Ning Xin. Yarn on yarn abrasion performance of high modulus polyethylene fiber improved by graphene/polyurethane composites coating. *Journal of Engineered Fibers and Fabrics*, 2021, 16.
7. Pylios T, Shepherd D E T. Prediction of lubrication regimes in wrist implants with spherical bearing surfaces. *Journal of Biomechanics*, 2004, 37 (3), 405-411.
8. Deng H, Wang L, Guo Y, Zhang Y, Wang C. Analysis of the Hydrodynamic Lubrication Characteristics of the External Return Spherical Bearing Pair of an Axial Piston Pump/Motor. *Mathematical Problems in Engineering*, 2020, 2020, 1-14.
9. Agrawal N, Sharma S C. Performance of textured spherical thrust hybrid bearing operating with shear thinning and piezoviscous lubricants. *Proceedings of the Institution of Mechanical Engineers, Part J: Journal of Engineering Tribology*, 2021.
10. Wang J, Shen J F, Fan Y W. Static characteristics analysis of spherical hybrid sliding bearings. *Industrial Lubrication and Tribology*, 2019, 72 (1), 93-100.
11. Kumar J V, Rao R R. Effects of Surface Roughness in Squeeze Film Lubrication of Spherical Bearings. *Procedia Engineering*, 2015, 127, 955-962.
12. Huang F, Yang X, Zhu J, Xu J. Effect of surface texture distribution parameters on hydrodynamic lubrication and numerical optimization. *Journal of Physics*, 2020.
13. Ji Y, Yang Z, Ran J, Li H. Multi-objective parameter optimization of turbine impeller based on RBF neural network and NSGA-II genetic algorithm. *Energy Reports*, 2021, 7, 584-593.
14. Unal M, Onat M, Demetgul M, Kucuk H. Fault diagnosis of rolling bearings using a genetic algorithm optimized neural network. *Measurement*, 2014, 58, 187-196.
15. Rajeswara Rao B, Tiwari R. Optimum design of rolling element bearings using genetic algorithms. *Mechanism and Machine Theory*, 2007, 42 (2), 233-250.
16. Jat A, Tiwari R. Multi-objective optimization of spherical roller bearings based on fatigue and wear using evolutionary algorithm. *Journal of King Saud University - Engineering Sciences*, 2020, 32 (1), 58-68.

17. Gupta S, Tiwari R, Nair S B. Multi-objective design optimisation of rolling bearings using genetic algorithms. *Mechanism and Machine Theory*, 2007, 42 (10), 1418-1443. 355
356
18. Goenka P K, Booker J F. Spherical Bearings: Static and Dynamic Analysis Via the Finite Element Method. *Journal of Tribology*, 1980, 102 (3), 308-319. 357
358
359